Characterization of Fischer–Tropsch cobalt-based catalytic systems (Co/SiO_2 and Co/Al_2O_3) by X-ray diffraction and magnetic measurements

P. Dutta[1], N.O. Elbashir[2], A. Manivannan[1], M.S. Seehra,[1,*] and C.B. Roberts[2]

[1]*Physics Department, West Virginia University, Morgantown, WV 26506-6315, USA*
[2]*Department of Chemical Engineering, Auburn University, Auburn, AL 36849, USA*

Received 31 July 2004; 19 August 2004

Results of the characterization of six Co-based Fischer–Tropsch (FT) catalysts, with 15% Co loading and supported on SiO_2 and Al_2O_3, are presented. Room temperature X-ray diffraction (XRD), temperature and magnetic field (H) variation of the magnetization (M), and low-temperature (5 K) electron magnetic resonance (EMR) are used for determining the electronic states (Co^0, CoO, Co_3O_4, Co^{2+}) of cobalt. Performance of these catalysts for FT synthesis is tested at reaction temperature of 240 °C and pressure of 20 bars. Under these conditions, 15% Co/SiO_2 catalysts yield higher CO and syngas conversions with higher methane selectivity than 15% Co/Al_2O_3 catalysts. Conversely the Al_2O_3 supported catalysts gave much higher selectivity towards olefins than Co/SiO_2. These results yield the correlation that the presence of Co_3O_4 yield higher methane selectivity whereas the presence of Co^{2+} species yields lower methane selectivity but higher olefin selectivity. The activities and selectivities are found to be stable for 55 h on-stream.

KEY WORDS: cobalt catalysts; Fischer–Tropsch synthesis; magnetization; X-ray diffraction.

1. Introduction

Fischer–Tropsch synthesis (FTS) continues to receive attention as an alternative for the production of ultra-clean transportation fuels, chemicals, and other hydrocarbon products through the heterogeneous catalytic conversion of readily available syngas (CO/H_2) resources. Diesel fractions from FTS have unique characteristics that include very low sulfur and aromatic content, high cetane index and exceptional clean burning in compression-ignition engine. Compared to crude oil derived diesel, FTS diesel fuel has been shown to reduce the emissions of carbon monoxide, nitrogen oxides, hydrocarbons and other particulates. More important for the FTS process is that it can take full use of rich sources of natural gas and coal as a supplement to decreasing oil resources. Cobalt-based catalysts are known to provide the best compromise between performance and cost for the synthesis of hydrocarbons from syngas (CO/H_2 mixtures). Cobalt catalysts were also found to give the highest yields and longest lifetime producing mainly linear alkanes (paraffins) [1]. Since cobalt catalysts are not inhibited by the water-gas-shift (WGS), it gives a high productivity at high syngas conversion [2]. Optimum catalysts with high cobalt concentration and site density can be prepared by controlled reduction of nitrate precursors introduced via melt or aqueous impregnation methods [3]. Most of the industrial cobalt-based catalytic systems used in the FTS reaction are supported on either Al_2O_3 or SiO_2. Therefore, cobalt dispersion on the supported catalyst surface [4] and the interaction of the Co with the metal oxide support that affect the electronic density as well as the structure of the metal crystallites [5] are assumed to play significant role on the catalyst performance measured by the hydrocarbon selectivity (C_{5+}) and the catalyst activity. In this study, X-ray diffraction, magnetic and electron magnetic resonance (EMR) measurements, and surface area measurements are used to characterize three supported cobalt-based catalytic systems (low surface area (LSA) 15% Co/SiO_2, high surface area (HSA) 15% Co/SiO_2, and 15% Co/Al_2O_3). These catalytic systems were used in a conventional gas-phase FTS study conducted in a fixed-bed-reactor. The structure sensitivity of these catalysts is correlated to their activity and selectivity in the synthesis of CO and H_2. Another important objective of this study is to provide a detailed characterization of the structure and valence state of cobalt and the surface composition of those catalysts in a fresh form (i.e. after preparation), after calcination (calcined samples), and after use in the reaction (used sample).

2. Experimental

2.1. Catalysts preparation and surface area characterization

Three cobalt-based catalytic systems were investigated in this study. The alumina supported catalyst (15% Co/Al_2O_3) is a commercial catalyst purchased from United Catalysts. The two silica supported catalysts (15% Co/

*To whom correspondence should be addressed.
E-mail: mseehra@wvu.edu

1011-372X/04/1200–0203/0 © 2004 Plenum Publishing Corporation

SiO_2) were prepared using the impregnation technique. Highly pure fumed silica (99.8%) purchased from Aldrich was used to support the cobalt catalyst. The LSA-15% Co/SiO_2 catalyst was supported on a 200 m^2/g surface area fumed SiO_2, while the HSA-15% $Co/SiO_2$was supported on a 380 m^2/g surface area fumed SiO_2. The cobalt precursor is highly pure (98%) cobalt nitrate $Co(NO_3)_2{\cdot}6H_2O$ and was purchased from Aldrich Chemical Co. In a typical preparation procedure, a total amount of 74.31 g of the cobalt nitrate precursor was dissolved in 250 ml of distilled water while stirring at room temperature. After a clear solution was formed, the addition of 40 g of the support SiO_2 was commenced bit by bit while stirring. This step is very important to avoid formation of large particles during the mixing process. The mixture was then continuously stirred for more than 48 h at room temperature until a heavy paste was formed. The paste was then dried in an oven at 110 °C for about 4 h. The sample was then crushed into a powder (100–150 μm) and stored as a fresh catalyst sample. The catalyst powder was then calcined (calcined sample) in air environment at 400 °C in a special rotary oven (temperature programming of the oven is 3 K/min) for about 4 h.

The BET surface area of the calcined silica supported catalysts (LSA and HSA), and the alumina supported catalyst was measured by N_2 physisorption using a TriStar 3000 gas adsorption analyzer of high-quality surface area and porosimetry measurements. The surface area measurements of those catalysts were certified by Micromeritics Co. The analytical technique for BET surface area is as follows: a sample of our catalyst was first contained in an evacuated sample tube and cooled (typically) to cryogenic temperature, and then it was exposed to analysis gas at a series of precisely controlled pressures. With each incremental pressure increase, the number of gas molecules adsorbed on the surface increases. The equilibrated pressure (P) is compared to the saturation pressure (P_0) and their relative pressure ratio (P/P_0) is recorded along with the quantity of gas adsorbed by the sample at each equilibrated pressure. The BET surface area was then measured from the plot of $1/Q[(P_0/P)\text{-}1]$ versus the relative pressure P/P_0, where Q is the quantity adsorbed in (cm^3/g STP). The measured BET surface areas of the calcined samples are listed in Table 1.

2.2. Sampling and characterization procedures

In Table 1, the six catalysts investigated in this work are listed. These include fresh Co/SiO_2 catalysts A1 (HSA-15% Co/SiO_2) and B1 (LSA-15% Co/SiO_2) and their calcined forms A1/C and B1/C. The remaining two catalysts are: C1 which is 15% Co/Al_2O_3 (used as received from United Catalyst) and C1/U which is C1 used for 12 days in FTS experiments. Room temperature X-ray diffraction (XRD) patterns of these catalysts were obtained with a Rigaku diffractometer using CuK_α radiation with $\lambda = 0.15418$ nm. Measurements of magnetization M versus T and H were done with a commercial SQUID (superconducting quantum interference devices) magnetometer. EMR studies were carried out at the X-band frequency of 9.279 GHz with a variable temperature cryostat from Oxford Instruments. In this system, the microwave cavity remains at room temperature whereas the sample temperature can be varied from 4 to 300 K. In the EMR resonance condition $hf = g\mu_B H_0$, the microwave frequency f is accurately measured by a frequency counter and the resonance field H_0 by a NMR probe. The g-value can then be calculated using the standard values of the Planck's constant h and Bohr magneton μ_B. The magnetic field is modulated at 100 kHz so that the experimental traces represent dP/dH versus H, with P being the power absorbed.

2.3. Fischer–Tropsch study

The FTS experiments were conducted in a high pressure stainless steel fixed-bed-reactor that composed of three sections as shown in Figure 1. The first section involves a syngas (H_2/CO mixture of ratio 2/1) delivery section, the second one involves the reaction section and the last one involves the product separation and analysis section. The first two sections are under controlled temperature (by using controlled heating tapes for the lines and temperature programmed furnace for the catalyst bed) and pressure (by using a back-pressure-regulator). The reactant, syngas, is delivered to the reaction zone through a mass flow controller (Brooks 5850E). The syngas cylinder is certified by Air Gas Company and it is composed of 31.2 volume% CO, 2.02 volume% N_2 and the balance is H_2. N_2 served as a

Table 1
Results of characterization of the cobalt-based catalytic systems

Sample	Description	BET Surface Area (m^2/g)	XRD	Magnetic	EMR
A1	15% HSA Co/SiO_2-Fresh	–	SiO_2	Curie-Weiss, Co^{2+}	Co^{2+}-line, $g \approx 4.3$
B1	15% LSA Co/SiO_2-Fresh	–	SiO_2	Curie-Weiss, Co^{2+}	Co^{2+}-line, $g \approx 4.3$
A1/C	Calcined A1	256	SiO_2, Co_3O_4	Co_3O_4	No line
B1/C	Calcined B1	158	SiO_2, Co_3O_4	Co_3O_4	Co^{2+}-weak line, $g \approx 4.3$
C1/C	15%Co/Al_2O_3-calcined	95	Co_3O_4, δ-Al_2O_3	Co_3O_4	Co^{2+}-line, $g \approx 4.3$ with sharp line
C1/U	C1 used in FTS reaction for 12 days	–	Co_3O_4, $Al_2O_3(\alpha, \delta, \chi)$	Co^0, Co^{2+}	Co^{2+}-line. Co^0-line

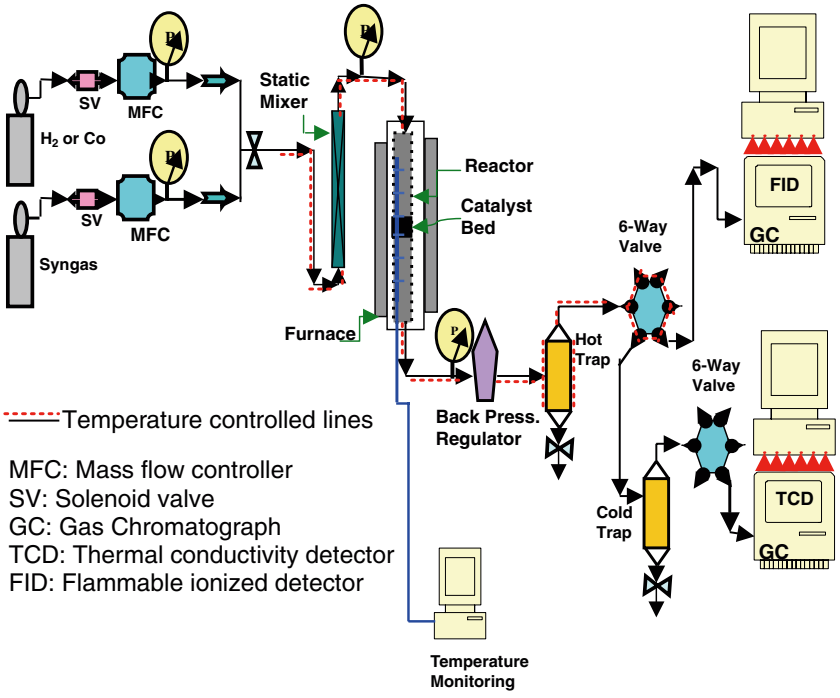

Figure 1. High pressure Fischer–Tropsch synthesis reactor and analysis system.

reference gas to aid in the chromatographic analysis and in the calculations of the activity and selectivity. The high pressure reactor (purchased from HIP) is a conventional down-flow fixed-bed stainless steel reactor with effective volume of 32 cm^3. One gram of the cobalt-based catalyst was supported on a titanium disc that was fixed in the middle of the reactor. Detailed description of the unit and the gas chromatograph analysis of reactants and products as well as the control of the operation modes are provided elsewhere [6,7].

Before using the catalyst in the reaction two methods of pretreatment were conducted. The alumina supported catalyst was pretreated in CO environment (50 sccm) at 280 °C for 18 h, while the silica supported catalysts were reduced in H_2 environment (100 sccm) at 340 °C for 4 h. The flow rate of syngas (H_2/CO ratio of 2) was fixed at 50 sccm, unless otherwise mentioned.

3. Results and Discussion

3.1. Background theory for magnetic studies

In order to provide a basis for the interpretation of the magnetic data, we briefly outline the theoretical expressions used in the analysis. We have measured the magnetization M against temperature T from 2 to 350 K at a fixed field $H = 100$ Oe and the magnetization M versus H at 2 K for H upto 55 kOe. For a paramagnetic system, the magnetic susceptibility $\chi = M/H$ is expected to follow the Curie–Weiss law given by [8]

$$\chi = \chi_0 + \frac{C}{T-\theta} \tag{1}$$

where the constants χ_0, C and θ are determined from the fit. The Curie constant $C = Ng^2\mu_B^2 S(S+1)/3\ k_B$ with N being the number of paramagnetic ion, g is the electronic g-value with spin S and μ_B and k_B are respectively the Bohr magneton and the Boltzmann constant. The Curie-temperature θ measures the exchange interaction between the neighboring paramagnetic ions, $\theta > 0$ for ferromagnetic and $\theta < 0$ for antiferromagnetic interactions. χ_0 includes the diamagnetic and other contribution of the lattice and the bonds. Knowing g and S, and experimental C, the concentration N of the paramagnetic ions can be determined.

The magnetization M of an assembly N of paramagnetic ions with the applied field H is also expected to vary according to the Brillouin function $B_S(x)$ [8,9]:

$$\frac{M}{M_0} = B_S(x) = \frac{2S+1}{2S}\coth\left(\frac{2S+1}{2S}x\right) - \frac{1}{2S}\coth\left(\frac{x}{2S}\right) \tag{2}$$

where $x = g\mu_B SH/k_B T$ and $M_0 = Ng\mu_B S$ is the magnetization of a perfectly aligned system of N ions, each with moment $= g\mu_B S$. Since this occurs only at absolute zero for a paramagnetic system, the M versus H measurements must be carried out at the lowest possible temperature, $T = 2$ K for our experiments. This analysis provides the magnitudes of g, S and M_0 and hence the magnitude of N. The two measurements combined yields the electronic state of the paramagnetic ion from the magnitude of g and S and the concentration from N. A peak in the χ versus T is usually observed in systems due to a magnetic transition. For CoO and Co_3O_4, this transition to antiferromagnetic ordering

occurs near $T_N = 290$ K [10] and $T_N \approx 40$ K [11] respectively. Elemental Co^0 is a ferromagnet with the Curie ordering temperature T_C well above room temperature ($T_C = 1388$ K) [8], so at room temperature hysteresis loop should be observed if Co^0 is present.

3.2. X-ray diffraction and magnetic studies

3.2.1. Fresh samples

The room temperature XRD patterns of the fresh samples A1 and B1 are shown in Figure 2. The broad line centered around $2\theta \approx 24^0$ is due to the SiO_2 [12]. No peaks due to crystalline phases are observed indicating that in 15% Co/SiO_2, Co is not present in any of its usual forms such as Co^0, CoO or Co_3O_4. Further confirmation of this comes from the χ versus T data discussed next.

The data of χ versus T for A1 and B1 samples measured with $H = 100$ Oe are shown in Figure 3 with the log-scale for the temperatures in order to give details of the low temperature data. The solid lines are fits to equation (1) with the parameters of the fit (χ_0, C and θ) given in Figure 3. The fits are excellent with negligible θ, showing that Co must be in the paramagnetic state, either as Co^{2+} or Co^{3+}, with the expected moment $\mu = gS$ equal to 3.3 for Co^{2+} and 4.4 for Co^{3+} [8] in the high spin states. To determine g and S for the present cases, the plot of M versus H at $T = 2$ K is fit to the Brillouin function (equation (2)) with $S = 3/2$ and $g = 2.2$ expected for Co^{2+} [8,11]. Excellent fits are obtained for both for the A1 and B1 samples (Figure 4) with the M_0 values given in Figure 4. Thus we conclude Co^{2+} in the high spin state to be the electronic state of cobalt in these samples. This state is possible for Co^{2+} surrounded by either tetrahedral or octahedral crystalline fields [11]. Thus Co^{2+} is either substituting for Si as in $Co_xSi_{1-x}O_2$ or perhaps chemisorbed on the surface of SiO_2 with bonding provided by surface absorbed H_2O and O_2.

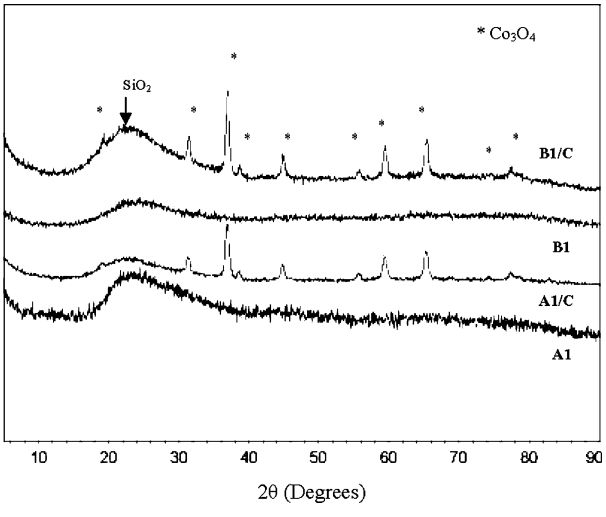

Figure 2. Room temperature XRD patterns of the catalysts shown using $\lambda = 0.15418$ nm. The Co_3O_4 and SiO_2 lines are identified.

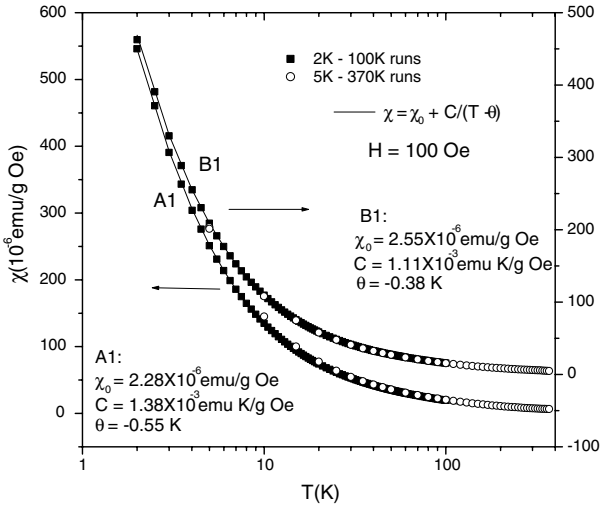

Figure 3. Temperature variations of the magnetic susceptibility χ for the A1 and B1 catalysts. The solid lines are fits to equation (1) with the magnitude of the parameters listed.

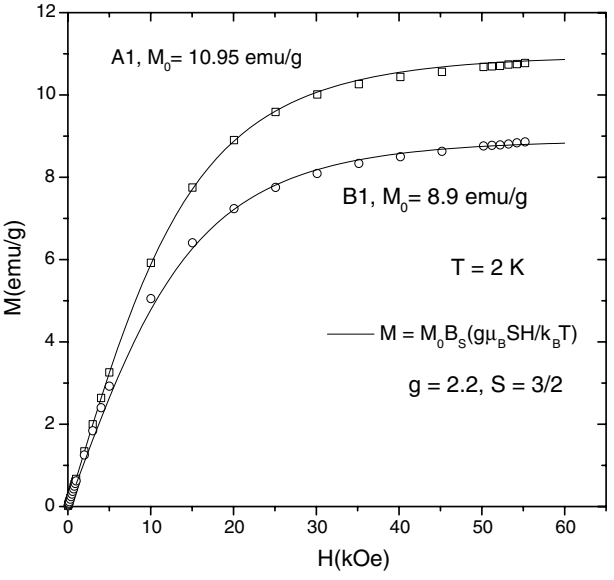

Figure 4. Magnetic field variations of the magnetization M at 2 K for the A1 and B1 samples. The solid lines are fits to equation (2) with the magnitudes of the parameters shown.

The concentration of Co^{2+} ions in the A1 and B1 samples can be calculated both from C and M_0 as discussed earlier. The two sets of calculated values are in excellent agreement and these are 3.7% for A1 and 3.0% for B1, much less the 15% nominal doping (The differences between the atomic and weight percentages of Co^{2+} in $Co_xSi_{1-x}O_2$ is negligible). A possible explanation for this large discrepancy between the nominal

and measured concentration is the presence of a part of Co in the Co^{3+} state in the low-spin configuration of $S = 0$, which occurs in strong octahedral crystalline field [11]. In this case Co^{3+} has no magnetic moments and hence not measured in the magnetic studies. This indeed is the case of for Co_3O_4 which contains both Co^{2+} and Co^{3+} configuration, the latter carrying no magnetic moment [11].

In summary then, while XRD provided a null result for Co^0, CoO and Co_3O_4 in the fresh samples, magnetic measurements yielded the presence of Co^{2+} ions in the range of around 3%, with the rest of Co perhaps in the low-spin Co^{3+} state. The detection of Co_3O_4 in the calcined samples discussed next confirms this characterization.

3.2.2. Calcined samples

The XRD patterns of the calcined samples A1/C and B1/C are also shown Figure 2. All the observed Bragg peaks can be identified with crystalline Co_3O_4 with the crystallite size $\approx$ 14 nm. The other oxide of cobalt viz. CoO is not observed. A similar result of the presence of Co_3O_4 is reported in Zr-promoted Co/SiO_2 [12]. Additional confirmation of the presence of Co_3O_4 and absence of CoO comes from the measurements of χ versus T shown in Figure 5. The observation of a peak in χ near the known $T_N \approx 40$ K of Co_3O_4 [11] in both A1/C and B1/C samples is a definite confirmation of the presence of Co_3O_4 in these samples. Comparing the magnitude of χ with that of pure Co_3O_4 [11], more of the Co in the A1/C sample is converted to Co_3O_4, as compared to that in B1/C, the latter having more of the background paramagnetic contribution thereby masking the peak at 40 K. There is no peak near the expected $T_N \approx 290$ K of CoO, thereby indicating the absence of CoO. The magnitude of χ in the A1/C sample is consistent with about 15% concentration of Co_3O_4. These observations agree with the conclusion drawn from the XRD results.

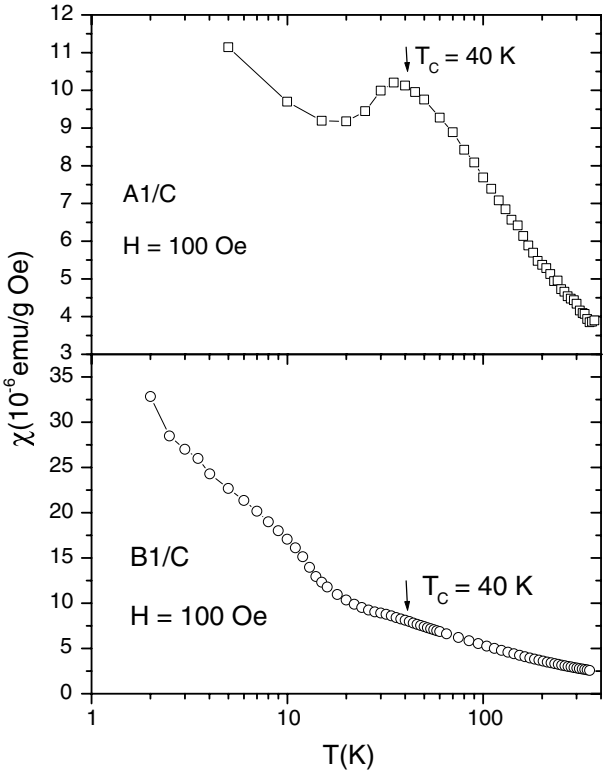

Figure 5. Temperature variation of the magnetic susceptibility χ for the A1/C and B1/C samples. $T_C = 40$ K represents the magnetic transition due to Co_3O_4.

3.2.3. Co/Al_2O_3 samples

The XRD patterns of the Co/Al_2O_3 based samples (C1/C and C1/U of Table 1) are shown in Figure 6. These results indicate that in the calcined but un-used sample C1/C, Co_3O_4 and Al_2O_3 (α, δ, χ) are present. After using the sample for 12 days in the reaction, Co_3O_4 is partly reduced to Co^0, whereas several different forms of Al_2O_3 are observed. The magnetic measurements shown in Figure 7 for C1/C do indicate the presence of Co_3O_4 since the signature anomaly of Co_3O_4 near 40 K is indicated. For C1/U, the χ versus T data shown in Figure 7 show considerably enhanced χ and behavior characteristic of magnetic nanoparticles as indicated by the bifurcation of the FC (field-cooled) and the zero-field-cooled (ZFC) data. The M versus H data at 300 K yields a hysteresis loop with coerceivity $H_C = 325$ Oe. The hysteresis loops measured at 5 K for C1/U cooled in $H = 0$ and $H = 20$ kOe from 300 K shows loop shift (Figure 8) to negative fields with exchange-bias $H_e = -42$ Oe. This is characteristic of a ferromagnetic/antiferromagnetic interface, in this case Co^0/Co_3O_4 [13]. The presence of Co^0 in the C1/U sample is barely evident from XRD since concentrations less than 1% are difficult to detect

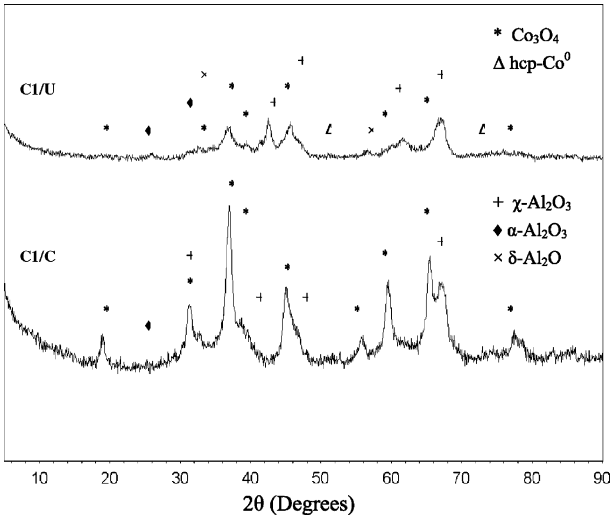

Figure 6. Room temperature XRD patterns of the C1/C and C1/U catalysts with the identified phases as shown.

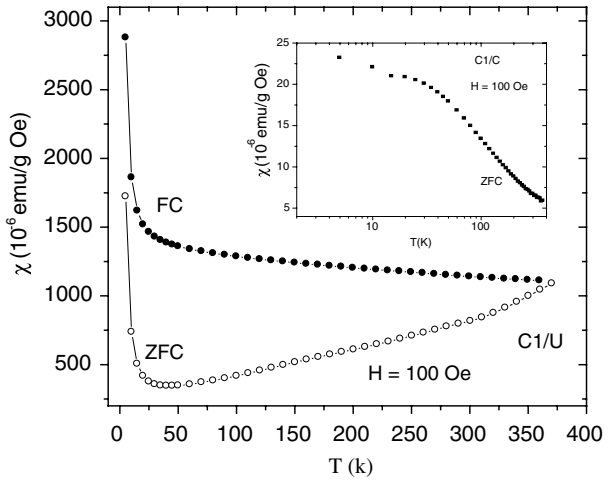

Figure 7. Temperature variations of the magnetic susceptibility χ for the C1/C (left scale) and C1/U (right scale) samples under ZFC (zero-field-cooled) and FC (field-cooled) conditions. The sharp rise in χ at low temperatures for C1/U is due to Co^{2+}.

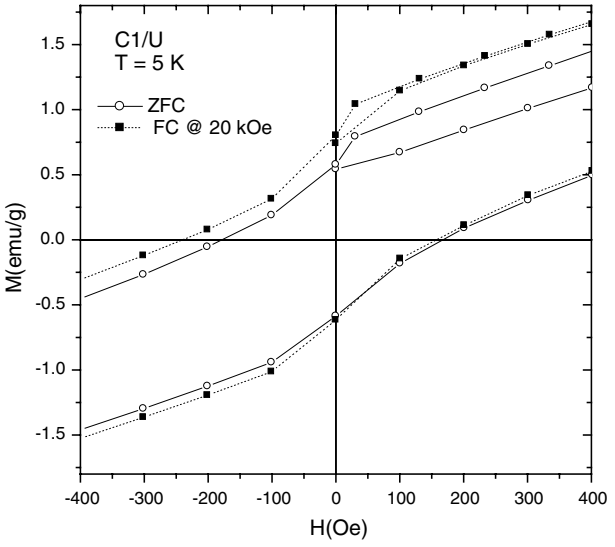

Figure 8. Low field part of the hysteresis loop data of magnetization versus applied field H for the ZFC and FC cases in C1/U. The shifted loop for the FC cases suggests Co^0/Co_3O_4 interface (see text).

by XRD. However, because of the large χ for Co^0 compared to that for CoO and Co_3O_4, even minute quantities of Co^0 are easily detected by magnetic measurements.

3.3. EMR characterization

The low temperature (5 K) EMR data (Figure 9) for the fresh samples A1 and B1 give a broad line at $g = 4.3$ due to Co^{2+} state [14]. The intensity of the EMR line decreases with increasing temperature. For the A1/C sample, an EMR line is not observed even at 5 K suggesting the absence of Co^{2+}. On the other hand, B1/C gives a weak line for $g = 4.3$ only at low temperature

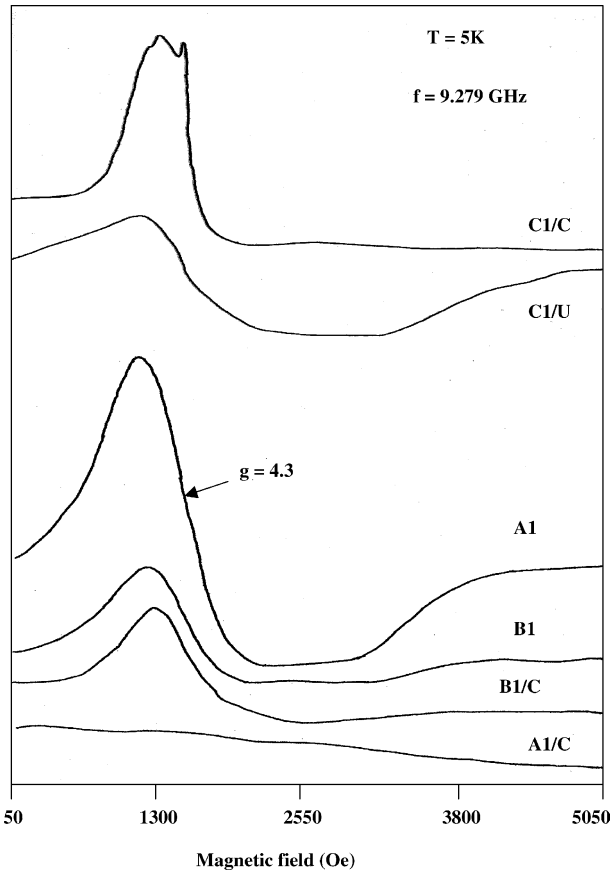

Figure 9. The EMR scans for various samples at temperatures shown.

and with increasing temperature the line becomes weaker and after 32 K it is not observed. These results suggest that in A1/C, cobalt is present only as Co_3O_4 whereas in B1/C, both Co_3O_4 and Co^{2+} are present. These results are consistent with the magnetic measurements shown in Figure 5.

In case of C1/C, we observe a line at $g = 4.3$ (Figure 9) due Co^{2+} superposed with another sharp line. The position of the line does not change with increasing temperature except the reduction of intensity. In the used sample (C1/U), the EMR data show the lines both for Co^{2+} ($g = 4.3$) and the broad line due to Co^0. These observations are consistent with the magnetic data shown in Figures 7 and 8.

4. Performance of the Cobalt-based Catalysts in Fischer–Tropsch Synthesis

The performance of the cobalt-based catalysts in FTS was tested in a high pressure reactor system under controlled temperature and pressure as shown in Figure 1. The reaction conditions and the set of operation modes were selected to mimic that of industrial conditions (favors high conversion rate of CO and H_2 per single pass at an acceptable chain growth probability of α-value above 0.60). Table 2 show the catalysts activity

Table 2
Activity and selectivity of three cobalt-based catalysts at 240 °C and pressure 20 ± 2 bar. H_2/CO ratio is two, and the syngas flowrate is 50 sccm/gcat

	Catalyst		
	A1/C	B1/C	C1/C
Activity			
CO Conversion (%)	83.2	87.9	76.8
Syngas (H_2+CO) conversion (%)	71.9	80.8	65.4
Selectivity			
CH_4 select (%)	21.3	18.9	16
CO_2 Select (%)	5.1	5.1	3.3
Alkanes select (%)[a]	63	66	58
Alkenes select (%)[a]	10.6	10	22.7
Chain growth probability			
α-value[b]	0.65	0.71	0.78

[a]Alkanes and alkenese selectivity include the isomers for hydrocarbon range of C2+

[b]The chain growth probability was determined from the slope of the best fitting line of the Andesron–Shultz–Flory distribution by using the following equation: $\ln(W_n/n) = n\ln\alpha + \ln[(1-\alpha)^2/\alpha]$ where W_n is the weight of hydrocarbons (paraffins, olefins and isomers) for a carbon number n. The heaviest hydrocarbon separated in our GC analysis is C_{30} and included in the a-value calculation is C_{35}

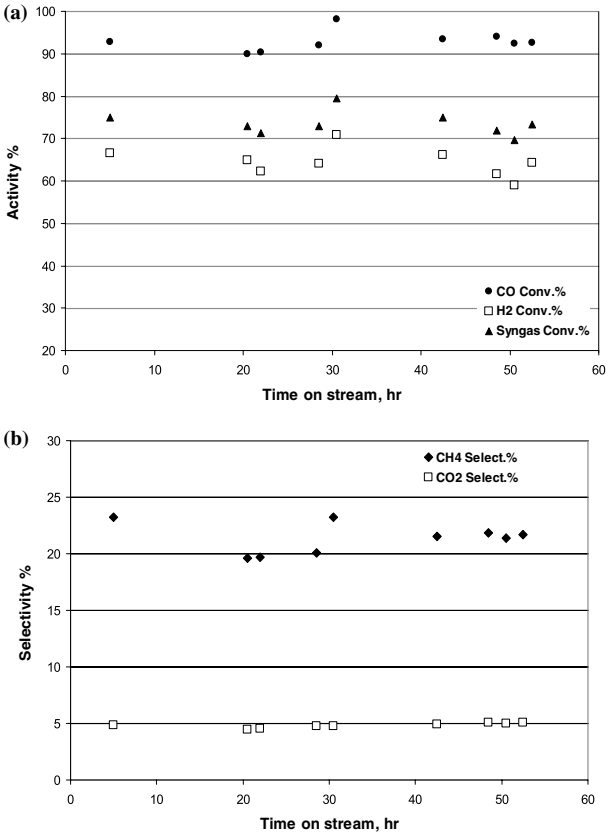

Figure 10. Percentage activities and selectivities of various fractions shown for the A1/C catalyst against time-on-stream in hours.

and selectivity at a reaction temperature of 240 °C and pressure of 20 ± 2 bar. The reported results in Table 2 have been collected after steady-state operation and prior to any deactivation of the catalyst taking place. A previous study has reported that the quasi steady state in reaction rates and selectivity of cobalt-based catalyst can be reached within as low as 4 h of time-on-stream (TOS) [15]. In the current study, the reported activity and selectivity is for samples analyzed after long times (c.a. 40 h TOS) to ensure stability of the catalysts under the studied conditions. Figure 10 shows an example of the A1/C catalyst stability with time on stream at relatively high reaction temperature of 250 °C. No significant changes (up to 55 h) in both activity (CO conversion, H_2 conversion and syngas conversion) and selectivity (CH_4 and CO_2) with TOS are observed as shown in Figure 10.

Under the studied conditions, the silica supported catalysts (A1/C and B1/C) were found to achieve higher CO and syngas conversions than the alumina supported one (C1/C) (see Table 1). This is also accompanied by higher methane selectivity of the silica supported catalysts (A1/C 21.3% and B1/C 18.9%) than that of the alumina supported one (C1/C 16%). In addition, the alumina supported catalyst (C1/C) gave much higher selectivity towards olefins (almost more than double of the silica supported ones, A1/C and B1/C). The C1/C catalyst also yields higher chain growth probability than the silica supported catalyst as shown in Table 1.

Initial inspection of the results suggests a correlation between the catalyst BET area and methane selectivity. A1/C catalyst has the highest surface area and shows the highest methane selectivity, followed by B1/C and C1/C. While a relation between catalyst surface area and methane selectivity has not been previously drawn, recent reports shows that the active phase reducibility of the cobalt catalyst is a function of the support's BET surface area [16]. Another characteristic that is known to give an indication of the methane selectivity is the size of Co particles [17]. The smaller the Co particles the higher would be the methane selectivity. Since the XRD pattern for the silica supported catalyst (A1/C and B1/C) showed almost the same crystallite size of Co_3O_4 (≈ 14 nm), one can not correlate the methane selectivity to the Co particle size from these results. Nevertheless, our EMR analysis shows interesting valence states of the cobalt particles on the catalyst surface. On the high surface area silica catalyst, A1/C, cobalt particles are present mainly as Co_3O_4 whereas in B1/C both Co_3O_4 and Co^{2+} are present on the catalyst surface. On the other hand, Co^{2+} is found to dominate the surface of the alumina supported catalyst (C1/C) and even after long use for12 days TOS under mild reaction conditions (up to 260 °C and 30 bar) stable forms of Co^{2+} still exist accompanied by Co^0. These observations are also consistent with magnetic data shown in Figure 7. As a result, lower methane selectivity accompanied by higher chain growth probability (α-value) and olefin selectivity

and in the case of C1/C can be attributed to the presence of stable form of Co^{2+}. This is in agreement with previous findings of many cobalt-based catalytic systems, whereas a direct correlation between the extent of reduction and the catalyst selectivity was drawn [17–20]. Khodakov *et al*. [17] reported that crystallite $Co_3O_4$was observed in all partially reduced catalysts (cobalt supported on mesoporous silica) of higher methane selectivity than the completely reduced. Reuel and Batholomew [18] suggested that the presence of stable unreduced oxide phases capable of catalyzing water-gas shift reaction will result in higher methane selectivity.

The other interesting result is the relatively higher CO and syngas conversions in the silica supported catalysts (A1/C and B1/C) compared to that of the alumina supported catalyst (C1/C). In a previous study Reuel and Batholomew [18] reported the activity of different cobalt-based catalytic systems and they ranked their catalysts in the following order: Co/TiO_2 >Co/Al_2O_3 >Co/SiO_2 >100% Co>Co/MgO. Such ranking indicates that alumina supported catalyst should yield higher activity than the silica supported one. Nevertheless, Igelsia *et al*. [5] have shown that the activity of cobalt catalysts is function of the metal dispersion and mostly independent of the type of support. Our results also showed that the lower surface area catalyst (B1/C) yield higher activity than the higher surface area catalyst (A1/C) which suggests no correlation between the catalyst surface area and its activity.

Acknowledgements

The authors would like to acknowledge the financial support of the Consortium for Fossil Fuel Science through U.S. Department of Energy, Contract No. DE-FC26-02NT41594, and Nippon Oil Corporation (Japan).

References

[1] P. Chaumette, C. Verdon and P. Boucot, Topics Catal 2 (1995) 301.
[2] P.J. Van Berge and R.C. Everson, Studies in Surface Science and Catalysis (Natural Gas Conversion IV) 107 (1997) 207.
[3] E. Iglesia, Appl. Catal. A: Gen. 161 (1997) 59.
[4] S.J. Tauster and S.C. Fung, J. Catal. 55 (1978) 29.
[5] E. Iglesia, S.L. Soled and R.A. Fiato, J. Catal. 137 (1992) 212.
[6] N.O. Elbashir and C.B. Roberts, *Ind. Eng. Chem. Res*. Submitted (2004).
[7] N.O. Elbashir and C.B. Roberts, Petrol. Chem. Div. Prep. 49 (2004) 157.
[8] C. Kittel, See e.g. *Introduction to Solid State Physics* by C. Kittel, 7th edn (John Wiley & Sons, NY, 1996).
[9] P. Dutta, A. Manivannan, M.S. Seehra, P.M. Adekkanattu and J.A. Guin, Catal. Lett. 94 (2004) 181.
[10] M.S. Seehra and P. Silinsky, Solid State Commun. 31 (1979) 183.
[11] W.L. Roth, J. Phys. Chem. Solids 25 (1964) 1.
[12] G.R. Moradi, M.M. Basir, Ataeb and A. Kiennemann, Catal. Commun. 4 (2003) 27.
[13] A.E. Berkowitz and K. Takano, J. Magn. Magn. Mater. 200 (1999) 552.
[14] W. Low, Phys. Rev. 109 (1958) 256.
[15] S. Sun, N. Tsubaki and K. Fujimoto, Appl. Catal. A: Gen. 202 (2000) 121.
[16] D.I. Enache, M. Roy-Auberger and R. Revel, Appl. Catal. A: Gen. In press (2004).
[17] A.Y. Khodakov, A. Griboval-Constant, R. Bechara and V.L. Zholobenko, J. Catal. 206 (2002) 230.
[18] R.C. Reuel and C.H. Batholomew, J. Catal. 85 (1984) 78.
[19] L. Fu and C.H. Bartholomew, J. Catal. 92 (1985) 376.
[20] B.S. Ernst, S. Libs, P. Chaumette and A. Kiennemann, Appl. Catal. A: Gen. 186 (1999) 145.